JOURNAL OF COMPUTATIONAL PHYSICS 122, 30–38 (1995)

A Multiscale Wavelet Solver with $O(n)$ Complexity

JOHN R. WILLIAMS AND KEVIN AMARATUNGA

Intelligent Engineering Systems Laboratory, Massachusetts Institute of Technology, Cambridge, Massachusetts 02139

Received January 3, 1994; revised February 2, 1995

In this paper, we use the biorthogonal wavelets recently constructed by Dahlke and Weinreich to implement a highly efficient procedure for solving a certain class of one-dimensional problems, $(\partial^{2l}/\partial x^{2l})u = f$, $l \in \mathbf{Z}$, $l > 0$. For these problems, the *discrete biorthogonal wavelet transform* allows us to set up a system of wavelet–Galerkin equations in which the scales are uncoupled, so that a true multiscale solution procedure may be formulated. We prove that the resulting stiffness matrix is in fact an almost perfectly diagonal matrix (the original aim of the construction was to achieve a block diagonal structure) and we show that this leads to an algorithm whose cost is $O(n)$. We also present numerical results which demonstrate that the multiscale biorthogonal wavelet algorithm is superior to the more conventional single scale orthogonal wavelet approach both in terms of speed and in terms of convergence. © 1995 Academic Press, Inc.

1. INTRODUCTION

Recent work by Dahlke and Weinreich [3] has resulted in a new construction which leads to families of biorthogonal wavelets ideally suited to solving problems of the form

$$\frac{\partial^{2l}}{\partial x^{2l}} u = f, \quad l \in \mathbf{Z}, l > 0.$$

The aim of the Dahlke–Weinreich construction is to obtain a scale-decoupled system of wavelet–Galerkin equations for such problems by forcing the stiffness matrix to be block diagonal. With orthogonal wavelets, there is insufficient freedom to achieve decoupling of the scales. The generalization to biorthogonal wavelets, however, provides the extra degrees of freedom needed. The Dahlke–Weinreich construction allows us to generate biorthogonal wavelets which exhibit the scale-decoupling property, using any orthogonal wavelet as a starting point.

We recall that the Daubechies orthonormal compactly supported wavelets [1] have arbitrarily high regularity; i.e., they may exactly represent polynomials of degree $N/2 - 1$, where N is the number of non-zero filter coefficients defining the scaling function. When the Dahlke–Weinreich construction is applied to Daubechies' wavelets, the resulting biorthogonal wavelets also exhibit smoothness which increases with N.

Here we outline our own numerical experiments using these new biorthogonal wavelets. We observe both numerically and theoretically that the resulting stiffness matrices for the above class of problems are not just block diagonal, but *almost perfectly diagonal*, under the application of the discrete biorthogonal wavelet transform. This allows us to develop an $O(n)$ solution procedure in which we solve for each of the scales separately. We implement the procedure and present convergence and cost results for our implementation.

In our discussion, we focus on problems with periodic boundary conditions. In Refs. [13, 14] we outline a capacitance matrix method which utilizes wavelet-based periodic solvers to enforce boundary conditions in elliptic boundary value problems. The general approach there is to use a *discrete analog* of the results of classical potential theory; e.g., for the Laplace equation on a planar region Ω, we would use a discrete form of the result

$$u(x) = \int_{\partial\Omega} \mu(\xi) \frac{\partial}{\partial n(\xi)} G(x - \xi)\, ds(\xi) \quad \text{or}$$

$$u(x) = \int_{\partial\Omega} \sigma(\xi) G(x - \xi)\, ds(\xi)$$

in which the *Green's function*, G, is calculated numerically using the periodic solver.

2. MULTIRESOLUTION ANALYSIS USING BIORTHOGONAL WAVELETS

2.1. *Biorthogonal Wavelet Bases*

We start by describing the setting for biorthogonal wavelets as a generalization of orthogonal wavelets. Biorthogonal wavelets are characterized by two sequences of embedded subspaces

$$\{0\} \cdots \mathbf{V}_{-2} \subset \mathbf{V}_{-1} \subset \mathbf{V}_0 \subset \mathbf{V}_1 \subset V_2 \cdots \mathbf{L}^2(\mathbf{R}),$$

$$\{0\} \cdots \tilde{\mathbf{V}}_{-2} \subset \tilde{\mathbf{V}}_{-1} \subset \tilde{\mathbf{V}}_0 \subset \tilde{\mathbf{V}}_1 \subset \tilde{\mathbf{V}}_2 \cdots \mathbf{L}^2(\mathbf{R}).$$

Two scaling functions are required: a primary scaling function, $\phi(x)$, for the subspaces $\mathbf{V}_m$ and a dual scaling function, $\tilde{\phi}(x)$, for the subspaces $\tilde{\mathbf{V}}_m$. Define the complementary spaces, $\mathbf{W}_m$ and $\tilde{\mathbf{W}}_m$, such that

$$\mathbf{V}_{m+1} = \mathbf{V}_m \oplus \mathbf{W}_m, \quad \tilde{\mathbf{V}}_{m+1} = \tilde{\mathbf{V}}_m \oplus \tilde{\mathbf{W}}_m, \tag{1}$$

0021-9991/95 $12.00

where $\oplus$ represents a *direct sum.* In general, the subspaces $\mathbf{V}_m$ and $\tilde{\mathbf{V}}_m$ are not orthogonal to their respective complements. Rather, they satisfy the conditions

$$\mathbf{W}_m \perp \tilde{\mathbf{V}}_m, \quad \tilde{\mathbf{W}}_m \perp \mathbf{V}_m. \tag{2}$$

The spaces $\mathbf{W}_m$ and $\tilde{\mathbf{W}}_m$ are generated from two wavelets, $\psi(x) \in \mathbf{W}_0$ and $\tilde{\psi}(x) \in \tilde{\mathbf{W}}_0$, respectively. Thus, conditions (2) imply that

$$\langle \psi(\cdot), \tilde{\phi}(\cdot - k) \rangle = 0, \quad \langle \tilde{\psi}(\cdot), \phi(\cdot - k) \rangle = 0. \tag{3}$$

In addition, we require that the primary and dual functions satisfy

$$\langle \phi(\cdot), \tilde{\phi}(\cdot - k) \rangle = \delta_{0,k}, \quad \langle \psi(\cdot), \tilde{\psi}(\cdot - k) \rangle = \delta_{0,k}. \tag{4}$$

The following scaling relations hold true

$$\phi(x) = \sum_k a_k \phi(2x - k), \quad \tilde{\phi}(x) = \sum_k \tilde{a}_k \tilde{\phi}(2x - k), \tag{5}$$

$$\psi(x) = \sum_k \tilde{b}_k \phi(2x - k), \quad \tilde{\psi}(x) = \sum_k b_k \tilde{\phi}(2x - k), \tag{6}$$

where the coefficient sequences are assumed to be of even length, N, and

$$b_k = (-1)^k a_{N-1-k}, \quad \tilde{b}_k = (-1)^k \tilde{a}_{N-1-k}.$$

Note that Eqs. (3) are automatically satisfied by the above defintions of b_k and $\tilde{b}_k$.

As with orthogonal wavelets, the non-vanishing integral of the scaling function leads to the constraints

$$\sum_k a_k = 2, \quad \sum_k \tilde{a}_k = 2. \tag{7}$$

In addition, Eq. (4) leads to the following condition on the filter coefficients:

$$\sum_k a_l \tilde{a}_{l-2k} = 2\delta_{0,k} \qquad \forall k \in \mathbf{Z}. \tag{8}$$

2.2. *Wavelets in the Fourier Domain*

Section 2.1 entailed a description of biorthogonal wavelets in the physical domain. This section summarizes their description in the Fourier domain. We use the notation

$$\hat{f}(\xi) = \int_{-\infty}^{\infty} f(x) e^{-i\xi x} dx$$

to denote the Fourier transform of $f(x)$.

Taking the Fourier transform of the scaling relations, Eqs. (5) and (6), leads to

$$\hat{\phi}(\xi) = \frac{1}{2} a(e^{-i(\xi/2)}) \hat{\phi}\left(\frac{\xi}{2}\right), \qquad \hat{\tilde{\phi}}(\xi) = \frac{1}{2} \tilde{a}(e^{-i(\xi/2)}) \hat{\tilde{\phi}}\left(\frac{\xi}{2}\right), \tag{9}$$

$$\hat{\psi}(\xi) = \frac{1}{2} \tilde{b}(e^{-i(\xi/2)}) \hat{\phi}\left(\frac{\xi}{2}\right), \qquad \hat{\tilde{\psi}}(\xi) = \frac{1}{2} b(e^{-i(\xi/2)}) \hat{\tilde{\phi}}\left(\frac{\xi}{2}\right), \tag{10}$$

where

$$a(e^{-i\xi}) = \sum_{k=0}^{N-1} a_k e^{-ik\xi}, \quad \tilde{a}(e^{-i\xi}) = \sum_{k=0}^{N-1} \tilde{a}_k e^{-ik\xi}, \tag{11}$$

$$b(e^{-i\xi}) = -e^{-i\xi(N-1)} \overline{a(-e^{-i\xi})}, \quad \tilde{b}(e^{-i\xi}) = -e^{-i\xi(N-1)} \overline{\tilde{a}(-e^{-i\xi})}. \tag{12}$$

Furthermore, Eq. (4) leads to the condition

$$\tfrac{1}{4}[a(e^{-i\xi}) \overline{\tilde{a}(e^{-i\xi})} + a(-e^{-i\xi}) \overline{\tilde{a}(-e^{-i\xi})}] = 1. \tag{13}$$

2.3. *The Discrete Biorthogonal Wavelet Transform*

The discrete biorthogonal wavelet transform (DBWT) is a straightforward generalization of the discrete wavelet transform (DWT). Since there are two sets of embedded subspaces $\{\mathbf{V}_m; m \in \mathbf{Z}\}$ and $\{\tilde{\mathbf{V}}_m; m \in \mathbf{Z}\}$, we define the respective projections of a function f onto these subspaces by

$$P_m f = \sum_k c_{m,k} \phi_{m,k}, \quad \text{and} \quad \tilde{P}_m f = \sum_k \tilde{c}_{m,k} \tilde{\phi}_{m,k}, \tag{14}$$

where $c_{m,k} = \langle f, \tilde{\phi}_{m,k} \rangle$ and $\tilde{c}_{m,k} = \langle f, \phi_{m,k} \rangle$. Likewise, we define the projections of f onto $\mathbf{W}_m$ and $\tilde{\mathbf{W}}_m$ by

$$Q_m f = \sum_k d_{m,k} \psi_{m,k}, \quad \tilde{Q}_m f = \sum_k \tilde{d}_{m,k} \tilde{\psi}_{m,k}, \tag{15}$$

where $d_{m,k} = \langle f, \tilde{\psi}_{m,k} \rangle$ and $\tilde{d}_{m,k} = \langle f, \psi_{m,k} \rangle$. By manipulating Eqs. (1), (3), (4), (5), and (6), we obtain the relations

$$c_{m,j} = \frac{1}{\sqrt{2}} \sum_k \tilde{a}_{k-2j} c_{m+1,k}, \quad d_{m,j} = \frac{1}{\sqrt{2}} \sum_k b_{k-2j} c_{m+1,k}, \tag{16}$$

$$c_{m+1,k} = \frac{1}{\sqrt{2}} \sum_j a_{k-2j} c_{m,j} + \frac{1}{\sqrt{2}} \sum_j \tilde{b}_{k-2j} d_{m,j}. \tag{17}$$

We refer to Eqs. (16) as the primary DBWT. The inverse transformation is then given by Eq. (17), which we refer to as the primary IDBWT. Expressions for the dual DBWT and its inverse may be obtained by interchanging the symbols $(\cdot)$ and $(\tilde{\cdot})$. Note that Eqs. (16) and (17) represent a *single stage* in the decomposition and reconstruction process. In order to obtain the complete transforms these equations must be applied recursively over all scales m.

Next, we give the matrix form of the primary and dual DBWTs and their inverses. We use the notation W_n to denote the matrix which operates on some n-dimensional vector $\mathbf{c}$ to

produce the *first stage* of its primary DBWT. Likewise, we use the notation $\tilde{W}_n$ for the first stage of the dual DBWT. Then Eqs. (16) and (17) imply

$$W_n = \begin{bmatrix} \tilde{H} \\ G \end{bmatrix}, \quad W_n^{-1} = [H^T \tilde{G}^T] = \tilde{W}_n^T,$$
$$\tilde{W}_n = \begin{bmatrix} H \\ \tilde{G} \end{bmatrix}, \quad \tilde{W}_n^{-1} = [\tilde{H}^T G^T] = W_n^T, \tag{18}$$

where

$$H = \frac{1}{\sqrt{2}} \begin{bmatrix} a_0 & a_1 & \cdots & a_{N-1} & 0 & 0 & \cdots & 0 & 0 \\ 0 & 0 & a_0 & a_1 & \cdots & a_{N-1} & \cdots & 0 & 0 \\ \cdots & \cdots & \cdots & \cdots & \cdots & \cdots & \cdots & \cdots & \cdots \\ a_4 & a_5 & \cdots & 0 & 0 & 0 & \cdots & a_2 & a_3 \\ a_2 & a_3 & \cdots & 0 & 0 & 0 & \cdots & a_0 & a_1 \end{bmatrix}_{(n/2)\times n},$$

$$G = \frac{1}{\sqrt{2}} \begin{bmatrix} b_0 & b_1 & \cdots & b_{N-1} & 0 & 0 & \cdots & 0 & 0 \\ 0 & 0 & b_0 & b_1 & \cdots & b_{N-1} & \cdots & 0 & 0 \\ \cdots & \cdots & \cdots & \cdots & \cdots & \cdots & \cdots & \cdots & \cdots \\ b_4 & b_5 & \cdots & 0 & 0 & 0 & \cdots & b_2 & b_3 \\ b_2 & b_3 & \cdots & 0 & 0 & 0 & \cdots & b_0 & b_1 \end{bmatrix}_{(n/2)\times n},$$

and $\tilde{H}$ and $\tilde{G}$ are similarly defined in terms of the filters $\{\tilde{a}_k\}$ and $\{\tilde{b}_k\}$, respectively.

To conclude this section, we make the following remarks.

1. The application of Eqs. (16) and (17) to finite length sequences leads to problems at the boundaries. One possible solution is to develop wavelets which are adapted to an interval on the real line. In this discussion, however, we assume that the sequences are either periodic or periodizable by a smooth extension. The structure of the matrices H, G, $\tilde{H}$, and $\tilde{G}$ reflect this assumption.

2. The DBWT differs from the orthogonal discrete wavelet transform in that W_n is not an orthogonal matrix, i.e., $W_n^{-1} \neq W_n^T$, in general. In the language of subband coding, this means that we cannot expect perfect reconstruction if we use the same FIR filters for decomposition and reconstruction. Perfect reconstruction now requires that we have four filters instead of the two that are required with orthogonal wavelets. This is illustrated in Fig. 1, in which we use the symbol $\mathbf{x}$ to denote the sequence x_k and $\bar{\mathbf{x}}$ to denote the time reversed sequence x_{-k}.

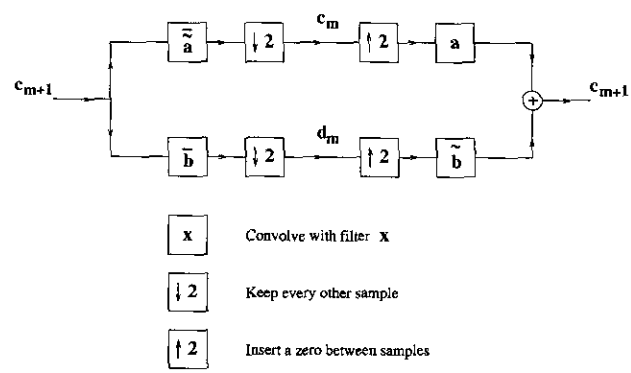

FIG. 1. Subband coding scheme for DBWT showing the use of different decomposition and reconstruction filters to obtain perfect signal reconstruction.

3. Finally, we note that the DBWT, like its orthogonal counterpart, is an $O(n)$ procedure. This is evident from a factorization of the matrix W_n into blocks as described in [2]:

$$W_n = \begin{bmatrix} odd\text{–}even \\ shuffle \end{bmatrix} \frac{1}{\sqrt{2}} \begin{bmatrix} \tilde{a}_0 & \tilde{a}_1 & \cdots & \tilde{a}_{N-1} & 0 & 0 & \cdots & 0 & 0 \\ b_0 & b_1 & \cdots & b_{N-1} & 0 & 0 & \cdots & 0 & 0 \\ 0 & 0 & \tilde{a}_0 & \tilde{a}_1 & \cdots & \tilde{a}_{N-1} & \cdots & 0 & 0 \\ 0 & 0 & b_0 & b_1 & \cdots & b_{N-1} & \cdots & 0 & 0 \\ \cdots & \cdots & \cdots & \cdots & \cdots & \cdots & \cdots & \cdots & \cdots \\ \tilde{a}_2 & \tilde{a}_3 & \cdots & 0 & 0 & 0 & \cdots & \tilde{a}_0 & \tilde{a}_1 \\ b_2 & b_3 & \cdots & 0 & 0 & 0 & \cdots & b_0 & b_1 \end{bmatrix}. \tag{19}$$

3. ADAPTATION OF WAVELETS TO DIFFERENTIAL OPERATORS

In this section we describe the Dahlke–Weinreich construction and we make some important observations regarding the properties of the resulting biorthogonal wavelets.

3.1. *The Dahlke–Weinreich Construction*

The motivation behind the Dahlke–Weinreich construction is to obtain a scale-decoupled system of equations when the wavelet–Galerkin method is applied to problems of the form

$$\frac{\partial^{2l}}{\partial x^{2l}} u = f, \quad l \in \mathbf{Z}, l > 0. \tag{20}$$

This decoupling of the scales would enable us to solve separately for the different scales (frequency bands) that occur in u.

Hitherto, the principles of multiresolution analysis have not been directly applicable to the solution of ODEs and PDEs because the application of the two-dimensional DWT to the

wavelet–Galerkin stiffness matrix does not in general produce a block diagonal matrix. With orthogonal wavelets, the requirement for a block diagonal matrix is that

$$\langle \phi^{(2l)}(\cdot),\ \psi(\cdot - k)\rangle = \langle \phi(\cdot),\ \psi^{(2l)}(\cdot - k)\rangle = 0.$$

However, it is not possible to generate filter coefficients which satisfy this condition since this would violate the orthogonality of the scaling function to the wavelet.

With biorthogonal wavelets, there are two conceivable options. One is to require that $\langle \phi^{(2l)}(\cdot),\ \tilde{\psi}(\cdot - k)\rangle = 0$. However, this condition would contradict Eq. (3). The second (and viable) option is to require that

$$\langle \phi^{(2l)}(\cdot),\ \psi(\cdot - k)\rangle = 0. \tag{21}$$

The Dahlke–Weinreich construction to achieve condition (21) is summarized as follows.

Construction 3.1. Let $\{h_k;\ k = 0 \cdots N\}$ be the filter associated with Daubechies N coefficient orthonormal compactly supported wavelet and let

$$q(e^{-i\xi}) \equiv 2m_0(\xi) = \sum_{k=0}^{N-1} h_k e^{-ik\xi} \tag{22}$$

be the corresponding transfer function. Then the transfer functions of the primary and dual biorthogonal scaling functions which satisfy (21) are given by

$$\begin{aligned} a(e^{-i\xi}) &= \left(\frac{1 + e^{-i\xi}}{2}\right)^l q(e^{-i\xi}), \\ \tilde{a}(e^{-i\xi}) &= \left(\frac{2e^{-i\xi}}{1 + e^{-i\xi}}\right)^l q(e^{-i\xi}). \end{aligned} \tag{23}$$

We refer to [3] for a proof of this construction. Our numerical experiments have shown that the Dahlke–Weinreich construction may be successfully applied to orthogonal wavelets other than the Daubechies wavelets. The resulting biorthogonal wavelets exhibit the same properties as those derived from the Daubechies wavelets.

3.2. *Properties of the Dahlke–Weinreich Wavelets*

Recall that the aim of the construction was to achieve

$$\langle \phi^{(2l)}(\cdot),\ \psi(\cdot - k)\rangle = 0.$$

In this section we highlight another important property of the Dahlke–Weinreich wavelets which arises naturally from their construction. It is this property which allows us to solve Eq. (20) in $O(n)$ time. The following result was initially observed in numerical experiments; a formal proof is given in Appendix A.

TABLE I

Filter Coefficients of the Biorthogonal Wavelets Adapted to $\partial^2/\partial x^2$ Which Are Derived from Daubechies D12 Wavelet

k	h_k	a_k	$\tilde{a}_k$
0	0.15774243200288	0.07887121600144	0.00000000000000
1	0.69950381407516	0.42862312303902	0.31548486400577
2	1.06226375988165	0.88088378697841	1.08352276414456
3	0.44583132293005	0.75404754140585	1.04100475561874
4	−0.31998659889202	0.06292236201902	−0.14934210975863
5	−0.18351806406025	−0.25175233147613	−0.49063108802541
6	0.13788809297474	−0.02281498554276	0.12359495990491
7	0.03892320970833	0.08840565134153	0.15218122604456
8	−0.04466374833018	−0.00287026931092	−0.07433480662789
9	0.00078325115230	−0.02194024858894	−0.01499269003246
10	0.00675606236293	0.00376965675761	0.01655919233706
11	−0.00152353380560	0.00261626427866	−0.00304706761120
12		−0.00076176690280	0.00000000000000
13		0.00000000000000	0.00000000000000

THEOREM 3.1. *Let ψ be the primary biorthogonal wavelet derived using the Dahlke–Weinreich construction. Then the $(2l)$th derivative of ψ satisfies the property*

$$\langle \psi^{(2l)}(\cdot),\ \psi(\cdot - k)\rangle = (-1)^l 2^{4l}\delta_{0,k},$$

where $\delta_{0,k}$ is the Kronecker delta.

Theorem 3.1 states that the primary wavelet, ψ, is orthogonal to its $(2l)$th derivative. The implication of this result is that the dual DBWT of the stiffness matrix is a *diagonal* matrix, with the exception of the low frequency block. The low frequency block consists of terms of the form $\langle \phi^{(2l)}(\cdot),\ \phi(\cdot - k)\rangle$ and it has been shown in [3] that

$$\langle \phi^{(2l)}(\cdot),\ \phi(\cdot - k)\rangle = \sum_{j=-l}^{l} \binom{2l}{j+l} (-1)^{j+l}\delta_{j,k}. \tag{24}$$

Note that these are exactly the coefficients of the corresponding finite difference stiffness matrix. In particular, when $l = 1$, we obtain the familiar centered difference scheme for the second derivative operator:

$$\langle \phi''(\cdot),\ \phi(\cdot - k)\rangle = \delta_{-1,k} - 2\delta_{0,k} + \delta_{1,k}. \tag{25}$$

Table I gives the filter coefficients of the biorthogonal wavelets adapted to $\partial^2/\partial x^2$, which are derived from the Daubechies 12 coefficient wavelet. Figure 2 shows the corresponding biorthogonal scaling functions and wavelets.

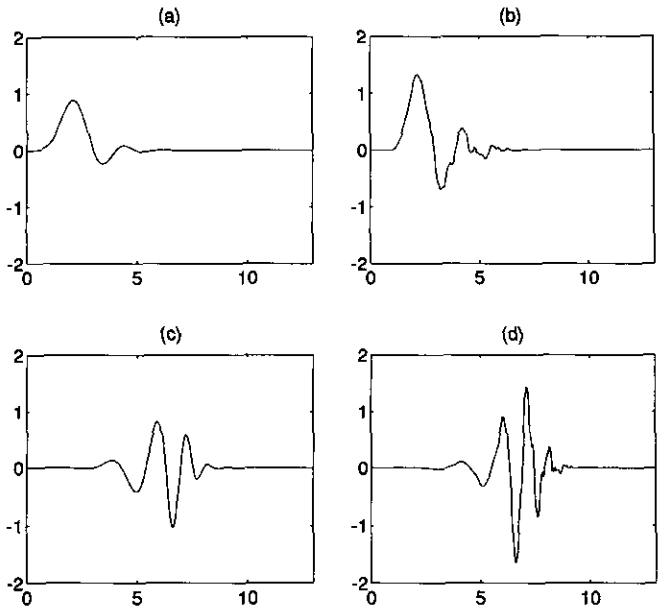

FIG. 2. Wavelets adapted to $\partial^2/\partial x^2$ and derived from Daubechies D12 wavelet: (a) Primary scaling function; (b) dual scaling function; (c) primary wavelet; (d) dual wavelet.

4. MULTISCALE WAVELET–GALERKIN SOLUTIONS IN $O(n)$ TIME

In this section, we describe how the Dahlke–Weinreich wavelets may be used to solve Eq. (20) in $O(n)$ time using a wavelet–Galerkin approach. Our discussion focuses on problems with periodic boundary conditions. An approach for applying wavelet–Galerkin periodic solvers to more general elliptic boundary value problems is described in [13, 14].

4.1. *The Wavelet–Galerkin Equations*

Consider the biorthogonal wavelet expansions

$$u_m(x) = \sum_{k=-\infty}^{\infty} c_{m,k}\phi_{m,k}(x), \quad f_m(x) = \sum_{k=-\infty}^{\infty} \tilde{s}_{m,k}\tilde{\phi}_{m,k}(x), \tag{26}$$

where the sequences $\{c_{m,k}\}$ and $\{\tilde{s}_{m,k}\}$ are n-periodic in k. Equivalently, the periodicity conditions on u_m and f_m are

$$u_m(x) = u_m(x + 2^{-m}n), \quad f_m(x) = f_m(x + 2^{-m}n).$$

Substituting in Eq. (20) and using $\{\tilde{\phi}_{m,j};\ j = 0, 1, \ldots, n-1\}$ as test functions, we get the wavelet–Galerkin equations

$$2^{2lm}\sum_{k=-\infty}^{\infty} c_{m,k}\langle\phi_{m,k}^{(2l)}, \tilde{\phi}_{m,j}\rangle = \tilde{s}_{m,j}, \quad j = 0, 1, \ldots, n-1; \tag{27}$$

i.e.,

$$2^{2lm}\begin{bmatrix} \Omega_0 & \Omega_{-1} & \cdots & \Omega_{-l} & \cdots & \Omega_l & \cdots & \Omega_1 \\ \Omega_1 & \Omega_0 & \cdots & \Omega_{1-l} & \cdots & 0 & \cdots & \Omega_2 \\ \cdots & \cdots & \cdots & \cdots & \cdots & \cdots & \cdots & \cdots \\ \Omega_l & \Omega_{l-1} & \cdots & \Omega_0 & \cdots & \cdots & \cdots & 0 \\ \cdots & \cdots & \cdots & \cdots & \cdots & \cdots & \cdots & \cdots \\ \Omega_{-l} & 0 & \cdots & \cdots & \cdots & \Omega_0 & \cdots & \Omega_{1-l} \\ \cdots & \cdots & \cdots & \cdots & \cdots & \cdots & \cdots & \cdots \\ \Omega_{-1} & \Omega_{-2} & \cdots & 0 & \cdots & \Omega_{l-1} & \cdots & \Omega_0 \end{bmatrix} \begin{bmatrix} c_{m,0} \\ c_{m,1} \\ c_{m,2} \\ \cdots \\ \cdots \\ \cdots \\ \cdots \\ c_{m,n-1} \end{bmatrix} = \begin{bmatrix} \tilde{s}_{m,0} \\ \tilde{s}_{m,1} \\ \tilde{s}_{m,2} \\ \cdots \\ \cdots \\ \cdots \\ \cdots \\ \tilde{s}_{m,n-1} \end{bmatrix}, \tag{28}$$

where

$$\Omega_k = \langle\phi_{m,0}^{(2l)}, \tilde{\phi}_{m,k}\rangle = \sum_{j=-l}^{l} \binom{2l}{j+l}(-1)^{j+l}\delta_{j,k}, \tag{29}$$

from Eq. (24). We abbreviate Eq. (28) to

$$K_m\mathbf{c}_m = \tilde{\mathbf{s}}_m. \tag{30}$$

4.2. *Decomposition of the Wavelet–Galerkin Equations*

We now consider a decomposition of u_m and f_m into components at scale $m-1$,

$$u_m = u_{m-1} + v_{m-1}, \quad f_m = f_{m-1} + g_{m-1}, \tag{31}$$

where

$$\begin{aligned} v_{m-1}(x) &= \sum_{k=-\infty}^{\infty} d_{m-1,k}\psi_{m-1,k}(x), \\ g_{m-1}(x) &= \sum_{k=-\infty}^{\infty} \tilde{t}_{m-1,k}\tilde{\psi}_{m-1,k}(x). \end{aligned} \tag{32}$$

Using the same test functions as before, the wavelet–Galerkin equations now become

$$2^{2l(m-1)} \sum_{k=-\infty}^{\infty} c_{m-1,k}\langle \phi_{m-1,k}^{(2l)}, \phi_{m,j}\rangle + 2^{2l(m-1)} \sum_{k=-\infty}^{\infty} d_{m-1,k}\langle \psi_{m-1,k}^{(2l)}, \phi_{m,j}\rangle$$

$$= \sum_{k=-\infty}^{\infty} \tilde{s}_{m-1,k}\langle \tilde{\phi}_{m-1,k}, \phi_{m,j}\rangle \qquad (33)$$

$$+ \sum_{k=-\infty}^{\infty} \tilde{t}_{m-1,k}\langle \tilde{\psi}_{m-1,k}, \phi_{m,j}\rangle, \quad j = 0, 1, \ldots, n-1.$$

Expanding $\phi_{m,j}$ using the relation

$$\phi_{m,j} = \frac{1}{\sqrt{2}} \sum_p \tilde{a}_{j-2p}\phi_{m-1,p} + \frac{1}{\sqrt{2}} \sum_p b_{j-2p}\psi_{m-1,p} \qquad (34)$$

and remembering that

$$\langle \phi_{m-1,k}^{(2l)}, \psi_{m-1,p}\rangle = \langle \psi_{m-1,k}^{(2l)}, \phi_{m-1,p}\rangle = 0,$$

we get

$$\frac{1}{\sqrt{2}} \sum_p \tilde{a}_{j-2p} 2^{2l(m-1)} \sum_{k=-\infty}^{\infty} c_{m-1,k}\langle \phi_{m-1,k}^{(2l)}, \phi_{m-1,p}\rangle$$

$$+ \frac{1}{\sqrt{2}} \sum_p b_{j-2p} 2^{2l(m-1)} \sum_{k=-\infty}^{\infty} d_{m-1,k}\langle \psi_{m-1,k}^{(2l)}, \psi_{m-1,p}\rangle \qquad (35)$$

$$= \frac{1}{\sqrt{2}} \sum_p \tilde{a}_{j-2p}\tilde{s}_{m-1,p} + \frac{1}{\sqrt{2}} \sum_p b_{j-2p}\tilde{t}_{m-1,p},$$

$$j = 0, 1, \ldots, n-1.$$

In matrix form Eq. (35) becomes

$$\tilde{W}_n^{-1} \begin{bmatrix} K_{m-1} & 0 \\ 0 & (-1)^l 2^{2l(m+1)} I_{n/2} \end{bmatrix} \begin{bmatrix} \mathbf{c}_{m-1} \\ \mathbf{d}_{m-1} \end{bmatrix} = \tilde{W}_n^{-1} \begin{bmatrix} \tilde{\mathbf{s}}_{m-1} \\ \tilde{\mathbf{t}}_{m-1} \end{bmatrix}, \qquad (36)$$

where we have used Theorem 3.1 to simplify $\langle \psi_{m-1,k}^{(2l)}, \psi_{m-1,p}\rangle$. Note that Eq. (36) is equivalent to Eq. (30).

Equation (36) tells us that the application of a single stage of the dual DBWT to Eq. (30) produces a system of equations in which the stiffness matrix is partially diagonalized. Applying further stages of the dual DBWT leads to a system with an *almost perfectly diagonal* stiffness matrix,

$$K_{\text{dec}}\mathbf{c}_{\text{dec}} = \tilde{\mathbf{s}}_{\text{dec}}, \qquad (37)$$

where $\mathbf{c}_{\text{dec}}$ and $\tilde{\mathbf{s}}_{\text{dec}}$ are the primary DBWT of $\mathbf{c}_m$ and the dual DBWT of $\tilde{\mathbf{s}}_m$, respectively, and K_{dec} is the 2D dual DBWT of K_m (obtained by applying the 1D transform to every column and then to every row). Since K_{dec} is almost perfectly diagonal, the solution of Eq. (37) requires no more than $O(n)$ operations. We recall that the DBWT and its inverse require $O(n)$ operations, so that the solution of Eq. (30) is also an $O(n)$ procedure.

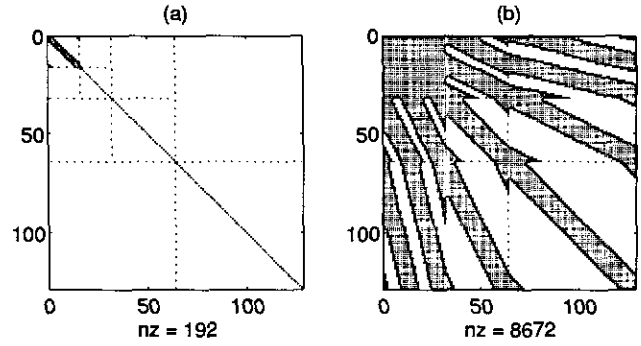

FIG. 3. Structure of the stiffness matrix for the operator $\partial^4/\partial x^4$ using (a) biorthogonal wavelets derived from D10 and (b) D10 orthogonal wavelets.

Figure 3a shows the sparse structure of the stiffness matrix, K_{dec}, for the operator $\partial^4/\partial x^4$ on the periodic interval [0, 1) with $m = 7$. The biorthogonal wavelets used to form the stiffness matrix were derived from Daubechies 10 coefficient wavelets. Figure 3b shows the structure of the stiffness matrix that would have been obtained if we used Daubechies 10 coefficient orthogonal wavelets instead.

4.3. *Scaling Function Coefficients and Expansions*

Finally, we need to determine the cost of evaluating the scaling coefficients of $f_m(x)$ and performing the expansion of $u_m(x)$ in Eq. (26). At first sight, the temptation might be to approximate the scaling coefficients by a discrete sampling of the functions f and u. Further thought reveals that such an approximation leads directly to Eq. (30), making the solution procedure equivalent to a conventional finite difference formulation of the problem. Thus, the high order of accuracy afforded by wavelets would be lost. To preserve high order accuracy while maintaining cost efficiency, we use the following procedures:

Evaluation of scaling function coefficients. The scaling function coefficients of $f(x)$ are given by a convolution integral:

$$\tilde{s}_{m,k} = \langle f(x), \phi_{m,k}\rangle = 2^{-ml/2} \int_{-\infty}^{\infty} f(2^{-m}y)\phi(y-k)\,dy. \qquad (38)$$

Suppose we are given n samples of $f(x)$, evenly spaced over one period:

$$f_j = f(2^{-m}j), \quad j = 0, 1, \ldots, n-1.$$

Then the scaling coefficients at the finest scale may be calculated from a discretization of Eq. (38),

$$\tilde{s}_{m,k} = 2^{-ml/2} \sum_{j=-\infty}^{\infty} f_j\phi(j-k), \qquad (39)$$

where $f_{j+n} = f_j$. Equation (39) leads to the system

$$\begin{bmatrix} \tilde{s}_{m,0} \\ \tilde{s}_{m,1} \\ \tilde{s}_{m,2} \\ \cdots \\ \cdots \\ \cdots \\ \cdots \\ \tilde{s}_{m,n-1} \end{bmatrix} = 2^{-m/2} \begin{bmatrix} \phi_0 & \phi_1 & \phi_2 & \cdots & \phi_{N_b-1} & \cdots & 0 & 0 \\ 0 & \phi_0 & \phi_1 & \cdots & \phi_{N_b-2} & \cdots & 0 & 0 \\ 0 & 0 & \phi_0 & \cdots & \phi_{N_b-3} & \cdots & 0 & 0 \\ \cdots & \cdots & \cdots & \cdots & \cdots & \cdots & \cdots & \cdots \\ \phi_{N_b-1} & 0 & 0 & \cdots & \cdots & \cdots & \phi_{N_b-3} & \phi_{N_b-2} \\ \cdots & \cdots & \cdots & \cdots & \cdots & \cdots & \cdots & \cdots \\ \phi_2 & \phi_3 & \phi_4 & \cdots & 0 & \cdots & \phi_0 & \phi_1 \\ \phi_1 & \phi_2 & \phi_3 & \cdots & 0 & \cdots & 0 & \phi_0 \end{bmatrix} \begin{bmatrix} f_0 \\ f_1 \\ f_2 \\ \cdots \\ \cdots \\ \cdots \\ \cdots \\ f_{n-1} \end{bmatrix}, \tag{40}$$

where N_b is the length of the biorthogonal wavelet filters. The values of the primary scaling function $\phi(x)$ for integer values of x are easily computed using by solving an eigenvalue problem arising from the dilation equation, Eq. (5) (see, e.g., [4] for details). From Eq. (40), it is evident that the scaling coefficients $\tilde{s}_{m,k}$ may be calculated in $O(n)$ operations.

Scaling function expansions. The evaluation of $u_m(x)$ in Eq. (26) also involves convolutions. This time, however, the procedure is exact. Consider n samples of $u_m(x)$, uniformly spaced over one period:

$$u_j = u_m(2^{-m}j), \quad j = 0, 1, \ldots, n-1.$$

From Eq. (26), we have

$$u_j = 2^{m/2} \sum_{j=-\infty}^{\infty} c_{m,k}\phi(j-k), \tag{41}$$

i.e.,

$$\begin{bmatrix} u_0 \\ u_1 \\ u_2 \\ \cdots \\ \cdots \\ \cdots \\ \cdots \\ u_{n-1} \end{bmatrix} = 2^{m/2} \begin{bmatrix} \phi_0 & 0 & 0 & \cdots & \phi_{N_b-1} & \cdots & \phi_2 & \phi_1 \\ \phi_1 & \phi_0 & 0 & \cdots & 0 & \cdots & \phi_3 & \phi_2 \\ \phi_2 & \phi_1 & \phi_0 & \cdots & 0 & \cdots & \phi_4 & \phi_3 \\ \cdots & \cdots & \cdots & \cdots & \cdots & \cdots & \cdots & \cdots \\ \phi_{N_b-1} & \phi_{N_b-2} & \phi_{N_b-3} & \cdots & \cdots & \cdots & 0 & 0 \\ \cdots & \cdots & \cdots & \cdots & \cdots & \cdots & \cdots & \cdots \\ 0 & 0 & 0 & \cdots & \phi_{N_b-3} & \cdots & \phi_0 & 0 \\ 0 & 0 & 0 & \cdots & \phi_{N_b-2} & \cdots & \phi_1 & \phi_0 \end{bmatrix} \begin{bmatrix} c_{m,0} \\ c_{m,1} \\ c_{m,2} \\ \cdots \\ \cdots \\ \cdots \\ \cdots \\ c_{m,n-1} \end{bmatrix}. \tag{42}$$

Thus $u_m(x)$ may be computed from its scaling coefficients in $O(n)$ time.

4.4. *Multiscale Solution Algorithm—Table II*

TABLE II

Multiscale Solution Algorithm

Compute the dual scaling function coefficients, $\tilde{\mathbf{s}}_m$, of $f(x)$.	$O(n)$
Compute the dual DBWT, $\tilde{\mathbf{s}}_{\text{dec}}$, of $\tilde{\mathbf{s}}_m$.	$O(n)$
Construct the stiffness matrix, K_{dec}, and solve for $\mathbf{c}_{\text{dec}}$.	$O(n)$
Apply the primary IDBWT to obtain the primary scaling function coefficients, $\mathbf{c}_m$, of $u_m(x)$.	$O(n)$
Expand $u_m(x)$ from its primary scaling function coefficients.	$O(n)$
Total cost	$O(n)$

5. NUMERICAL RESULTS

In this section, we present results from our implementation of the multiscale solution algorithm. We used three different

methods to solve the problem

$$\frac{\partial^2}{\partial x^2} u = -20\pi^2 \sin(2\pi x) \sin(4\pi x) + 16\pi^2 \cos(2\pi x) \cos(4\pi x), \tag{43}$$

where $u(x)$ is periodic with period 1 and has zero mean:

1. Multiscale solution of the decomposed wavelet–Galerkin equations (37) for the adapted biorthogonal wavelets derived from the Daubechies D6 wavelet. (Inversion of the coarsest scale stiffness matrix block was performed using the FFT.)

2. Direct solution of the wavelet–Galerkin equations (30) for the orthogonal Daubechies D6 wavelet. (Inversion of the stiffness matrix, K_m, was performed using the FFT.)

3. Direct solution of the wavelet–Galerkin equations (30) for the biorthogonal wavelets derived from the Daubechies D6 wavelet. (Inversion of the stiffness matrix, K_m, was performed using the FFT.)

Method 2 involves numerical calculation of the connection coefficients, $\langle \phi(\cdot), \phi(\cdot - k) \rangle$ (see [5]). The connection coefficients were precalculated and the cost of these computations is therefore not reflected in the results which follow.

Figure 4a compares the convergence of the three methods. Based on these numerical results, the multiscale algorithm and its equivalent single scale biorthogonal wavelet algorithm converge roughly as $O(\Delta x^{4.7})$, whereas the truncation error for the orthogonal wavelet algorithm is $O(\Delta x^{4.2})$. Note that higher order wavelets would have given higher rates of convergence while in contrast, a three-point finite difference scheme would converge only as $O(\Delta x^2)$. Algorithms 2 and 3 suffer from noise introduced by the FFT at large n as evidenced by the upturn in their curves. Clearly this problem is eliminated by the multiscale algorithm.

Finally, Fig. 4b compares the accuracy–cost performance of the three methods. This conclusively shows that the multiscale algorithm offers a considerable improvement in efficiency over the other two methods.

6. CONCLUSIONS

The construction of Dahlke and Weinreich opens new possibilities for the development of rapid and highly accurate solution procedures for ODEs and PDEs. We have shown that their construction leads to an almost perfectly diagonal stiffness matrix when the wavelet–Galerkin method is applied to a certain class of problems. This trivializes the task of inverting the stiffness matrix, allowing us to solve such problems in $O(n)$ time.

Work on adaptation of wavelets to more general differential operators as well as to higher dimensions has been done by Dahlke and Weinreich [6] and Dahlke and Kunoth [7]. The most important question now is whether these generalizations may be used to obtain $O(n)$ multiscale solutions for a larger class of problems.

APPENDIX A: PROOF OF THEOREM 3.1

$$\begin{aligned}
&\langle \psi^{(2l)}(\cdot), \psi(\cdot - k) \rangle \\
&= \int_{-\infty}^{\infty} \psi^{(2l)}(x) \overline{\psi(x-k)}\, dx \\
&= \frac{1}{2\pi} \int_{-\infty}^{\infty} \widehat{\psi^{(2l)}}(\xi) \overline{\hat{\psi}(x-k)}(\xi)\, d\xi \\
&= \frac{1}{2\pi} \int_{-\infty}^{\infty} (i\xi)^{2l} \hat{\psi}(\xi) \overline{e^{-ik\xi} \hat{\psi}}(\xi)\, d\xi
\end{aligned}$$

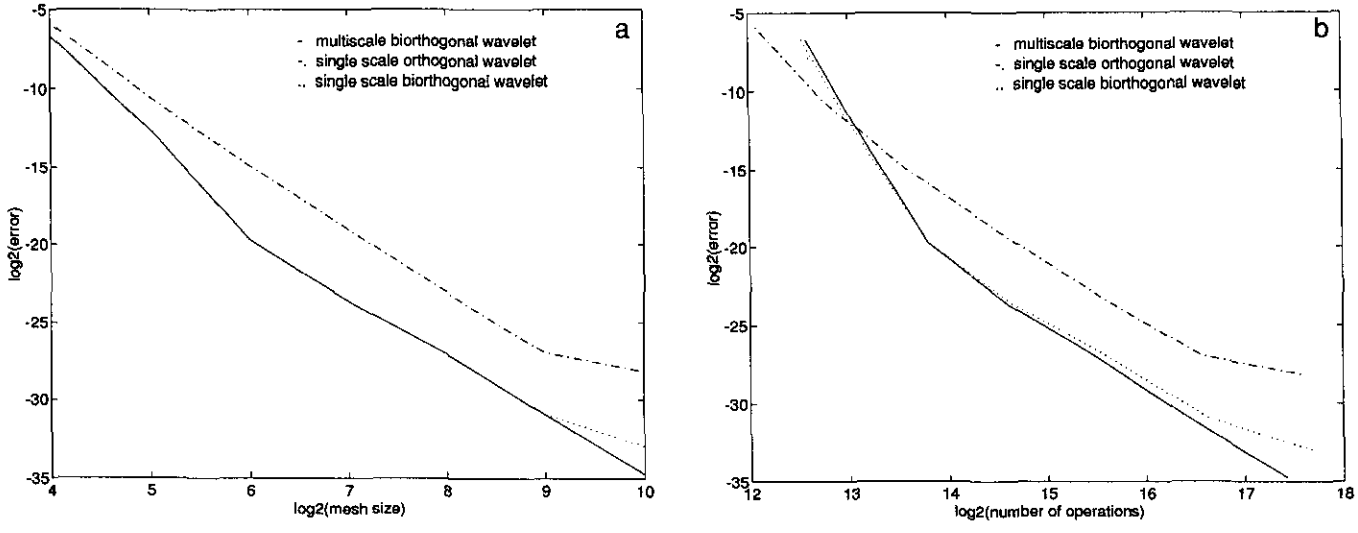

FIG. 4. (a) Error in computed solution. (b) Accuracy-cost performance of the three algorithms.

$$= (-1)^l \frac{1}{2\pi} \int_{-\infty}^{\infty} e^{ik\xi} \xi^{2l} \left[\frac{1}{2} \tilde{b}(e^{-i(\xi/2)}) \hat{\phi}\left(\frac{\xi}{2}\right) \right] \overline{\left[\frac{1}{2} \tilde{b}(e^{-i(\xi/2)}) \hat{\phi}\left(\frac{\xi}{2}\right) \right]} \, d\xi$$

$$= (-1)^l \frac{1}{8\pi} \int_{-\infty}^{\infty} e^{ik\xi} \xi^{2l} |\tilde{b}(e^{-i(\xi/2)})|^2 \left| \hat{\phi}\left(\frac{\xi}{2}\right) \right|^2 d\xi$$

$$= (-1)^l \frac{1}{8\pi} \int_0^{2\pi} e^{ik\xi} \sum_{n=-\infty}^{\infty} |\tilde{b}(e^{-i(\xi+2\pi n/2)})|^2 (\xi + 2\pi n)^{2l} \left| \hat{\phi}\left(\frac{\xi + 2\pi n}{2}\right) \right|^2 d\xi$$

$$= (-1)^l \frac{1}{8\pi} \int_0^{2\pi} e^{ik\xi} \left[|\tilde{b}(e^{-i(\xi/2)})|^2 \sum_{n=-\infty}^{\infty} (\xi + 4\pi n)^{2l} \left| \hat{\phi}\left(\frac{\xi + 4\pi n}{2}\right) \right|^2 + |\tilde{b}(-e^{-i(\xi/2)})|^2 \sum_{n=-\infty}^{\infty} (\xi + 2\pi + 4\pi n)^{2l} \left| \hat{\phi}\left(\frac{\xi + 2\pi + 4\pi n}{2}\right) \right|^2 \right] d\xi$$

$$= (-1)^l \frac{1}{8\pi} \int_0^{2\pi} e^{ik\xi} [|\tilde{b}(e^{-i(\xi/2)})|^2 g(\xi) + |\tilde{b}(-e^{-i(\xi/2)})|^2 g(\xi + 2\pi)] \, d\xi,$$

where from [3],

$$g(\xi) \equiv \sum_{n=-\infty}^{\infty} (\xi + 4\pi n)^{2l} \left| \hat{\phi}\left(\frac{\xi + 4\pi n}{2}\right) \right|^2 = 2^{2l} |1 - e^{-i(\xi/2)}|^{2l}. \tag{44}$$

Now

$$f(\xi) \equiv |\tilde{b}(e^{-i(\xi/2)})|^2 g(\xi) + |\tilde{b}(-e^{-i(\xi/2)})|^2 g(\xi + 2\pi)$$

$$= |-e^{-i(\xi/2)(N-1)} \overline{\tilde{a}(-e^{-i(\xi/2)})}|^2 g(\xi) + |e^{-i(\xi/2)(N-1)} \overline{\tilde{a}(e^{-i(\xi/2)})}|^2 g(\xi + 2\pi)$$

$$= |e^{-i(\xi/2)(N-1)}|^2 [|\tilde{a}(-e^{-i(\xi/2)})|^2 g(\xi) + |\tilde{a}(e^{-i(\xi/2)})|^2 g(\xi + 2\pi)]$$

$$= \left| \left(\frac{-2e^{-i(\xi/2)}}{1 - e^{-i(\xi/2)}} \right)^l q(-e^{-i(\xi/2)}) \right|^2 g(\xi) + \left| \left(\frac{2e^{-i(\xi/2)}}{1 + e^{-i(\xi/2)}} \right)^l q(e^{-i(\xi/2)}) \right|^2 g(\xi + 2\pi)$$

$$= \left| \left(\frac{-2e^{-i(\xi/2)}}{1 - e^{-i(\xi/2)}} \right)^l q(-e^{-i(\xi/2)}) \right|^2 2^{2l} |1 - e^{-i(\xi/2)}|^{2l} + \left| \left(\frac{2e^{-i(\xi/2)}}{1 + e^{-i(\xi/2)}} \right)^l q(e^{-i(\xi/2)}) \right|^2 2^{2l} |1 + e^{-i(\xi/2)}|^{2l}$$

$$= 2^{4l} |e^{-i(\xi/2)}|^{2l} [|q(-e^{-i(\xi/2)})|^2 + |q(e^{-i(\xi/2)})|^2]$$

$$= 2^{4l+2} \quad \text{since } |q(-e^{-i(\xi/2)})|^2 + |q(e^{-i(\xi/2)})|^2 = 4.$$

Thus we have

$$\langle \psi^{(2l)}(\cdot), \psi(\cdot - k) \rangle = (-1)^l \frac{1}{8\pi} \int_0^{2\pi} e^{ik\xi} f(\xi) \, d\xi = (-1)^l 2^{4l} \frac{1}{2\pi} \int_0^{2\pi} e^{ik\xi} \, d\xi = (-1)^l 2^{4l} \delta_{0,k}.$$

ACKNOWLEDGMENTS

This work was funded by a grant from NTT DATA Communications Systems Corporation, Kajima Corporation, and Shimizu Corporation to the Intelligent Engineering Systems Laboratory, Massachusetts Institute of Technology.

REFERENCES

1. I. Daubechies, *Comm. Pure Appl. Math.* **41,** 909 (1988).
2. G. Strang, "Wavelet Transforms versus Fourier Transforms," Department of Mathematics, Massachusetts Institute of Technology, 1992.
3. S. Dahlke and I. Weinreich, *Constr. Approx.* **9,** 237 (1993).
4. J. R. Williams and K. Amaratunga, *Int. J. Numer. Methods Eng.* **37,** 2365 (1994).
5. A. Latto, H. Resnikoff, and E. Tenenbaum, "The Evaluation of Connection Coefficients of Compactly Supported Wavelets," in *Proceedings, French–USA Workshop on Wavelets and Turbulence, Princeton Univ., June 1991* (Springer-Verlag, New York/Berlin, 1992).
6. S. Dahlke and I. Weinreich, *Appl. and Comput. Harmonic Analysis* **1**(3), 267 (1994).
7. S. Dahlke and A. Kunoth, Bericht Nr. 84, Institut für Geometrie und Praktische Mathematik, RWTH Aachen, April 1993.
8. S. G. Mallat, *IEEE Trans. Pattern Anal. Mach. Intel.* **11**(7), 674 (1989).
9. G. Beylkin, R. Coifman, and V. Rokhlin, *Comm. Pure Appl. Math.* **44,** 141 (1991).
10. G. Beylkin, R. Coifman, and V. Rokhlin, "Wavelets in Numerical Analysis," in *Wavelets and Their Applications,* edited by M. B. Ruskai (Jones & Bartlett, Boston, 1992).
11. J. Weiss, "Wavelets and the Study of Two Dimensional Turbulence," in *Proceedings, French–USA Workshop on Wavelets and Turbulence, Princeton Univ., June 1991,* edited by Y. Maday (Springer-Verlag, New York, 1992).
12. S. Qian and J. Weiss, *J. Comput. Phys.* **106**(1), 155 (1993).
13. K. Amaratunga, J. R. Williams, S. Qian, and J. Weiss, *Int. J. Numer. Methods Eng.* **37,** 2703 (1994).
14. K. Amaratunga and J. R. Williams, *Eng. Comput.* **10,** 4 (1993).